New Poly(butylene succinate)/Layered Silicate Nanocomposites. II. Effect of Organically Modified Layered Silicates on Structure, Properties, Melt Rheology, and Biodegradability

KAZUAKI OKAMOTO,[1] SUPRAKAS SINHA RAY,[2] MASAMI OKAMOTO[2]

[1]Nagoya Municipal Research Institute, Rokuban 3-4-41, Atsuta, Nagoya 456 0058, Japan

[2]Advanced Polymeric Materials Engineering, Graduate School of Engineering, Toyota Technological Institute, Hisakata 2-12-1, Tempaku, Nagoya 468 8511, Japan

Received 21 January 2003; revised 14 July 2003; accepted 15 July 2003

ABSTRACT: A series of new poly(butylene succinate) (PBS)/layered silicate nanocomposites were prepared successfully by simple melt extrusion of PBS and organically modified layered silicates (OMLS). Three different types of OMLS were used for the preparation of nanocomposites: two functionalized ammonium salts modified montmorillonite and a phosphonium salt modified saponite. The structure of the nanocomposites in the nanometer scale was characterized with wide-angle X-ray diffraction and transmission electron microscopic observations. With three different types of layered silicates modified with three different types of surfactants, the effect of OMLS in nanocomposites was investigated by focusing on four major aspects: structural analysis, materials properties, melt rheological behavior, and biodegradability. Interestingly, all these nanocomposites exhibited concurrent improvements of material properties when compared with pure PBS. © 2003 Wiley Periodicals, Inc. J Polym Sci Part B: Polym Phys 41: 3160–3172, 2003

Keywords: poly(butylene succinate); organically modified layered silicate; nanocomposites; structure; materials properties; melt rheology; biodegradable

INTRODUCTION

Throughout the world today, the development of biodegradable polymeric materials with excellent materials properties has been a subject of great research challenge in materials science. Aliphatic polyesters are among the most promising materials for the production of high-performance, environment-friendly biodegradable plastics. Biodegradation of aliphatic polyester is well known, in that some living microorganisms degrade them by producing enzymes that attack the polymer.[1] One of them is poly(butylene succinate) (PBS) of the trade name 'BIONOLLE'

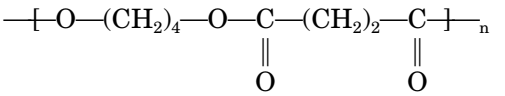

which is chemically synthesized by polycondensation of 1,4-butanediol with succinic acid. PBS is a commercially available, aliphatic thermoplastic polyester with many desirable properties including biodegradability, melt processability, and thermal and chemical resistance.[2] PBS has excel-

Correspondence to: M. Okamoto (E-mail: okamoto@toyota-ti.ac.jp)

Journal of Polymer Science: Part B: Polymer Physics, Vol. 41, 3160–3172 (2003)

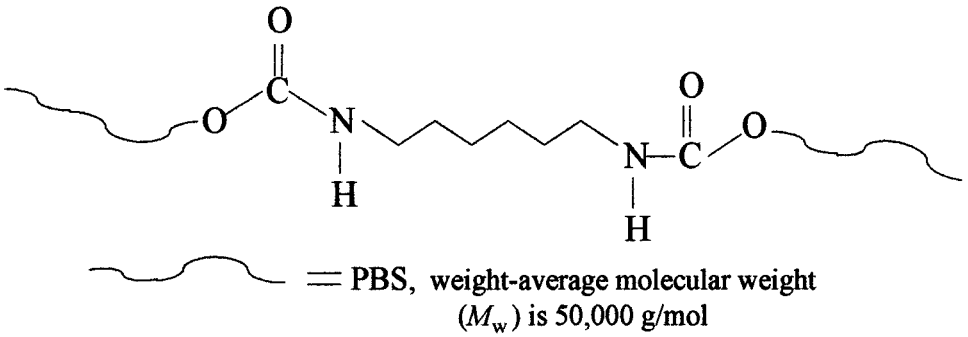

Scheme 1. Formation of urethane bonds in high-molecular-weight PBS.

lent processability and can be processed in the field of textiles into melt blow, multifilament, monofilament, nonwoven, flat and split yarn, and in the field of plastics into injection-molded products,[3] thus being a promising polymer for various potential applications. However, other properties of PBS, such as softness, tensile and gas-barrier properties, melt viscosity for further processing, and so forth, are frequently insufficient for various end-use applications.

In a natural extension of our ongoing research on biodegradable polylactide (PLA)/organically modified layered silicates (OMLS) nanocomposites (PLACNs),[4–12] we applied this nanocomposite technology to PBS to get material with improved materials properties suitable for a wide range of applications. In our previous research,[13] we reported on the preparation and characterization of intercalated PBS/octadecylammonium modified montmorillonite (C_{18}-MMT) nanocomposites.

This article first explores the preparation of PBS-based nanocomposites with three different types of OMLS. Second, the effect of OMLS on nanocomposites structure and morphology is investigated. Subsequently, we focus on a comparative study of the mechanical and tensile properties, oxygen gas permeability, and biodegradability of various nanocomposites. Finally, melt rheology of neat PBS and three different types of nanocomposites are examined.

EXPERIMENTAL

Materials

PBS (bionolle#1020) is a commercial product of Showa Denko (Japan) and was dried in an airflow oven before use. PBS was prepared by a coupling reaction of relatively low-molecular-weight PBS in the presence of hexamethylene diisocyanate (OCN-C_6H_{12}-NCO) as a chain extender. Each PBS chain had 0.48 wt % of chain extender, and this group made urethane-type bonds (as shown in Scheme 1) with hydroxy-terminated PBS having low molecular weight. Therefore, in the case of each high-molecular-weight PBS chain there was one diisocyanate unit at the middle of the polymer chain.[14,15]

Three different types of OMLS were synthesized by replacing Na^+ in different layered silicates with alkylammonium or alkylphosphonium cation by ion exchange. Table 1 presents the detailed specifications and designations (as written

Table 1. Specifications and Designation of OMLS

OMLS Codes	Pristine Clay	Particle Size (nm)	CEC (mequiv/100 g)	Organic Salts Used for the Modification of Pristine Clay	Supplier
C_{18}-MMT	Montmorillonite	150–200	110	Octadecylammonium cation	Nanocor Inc.
qC_{18}-MMT	Montmorillonite	100–130	90	Octadecyltrimethylammonium cation	Hojun Yoko Co.
qC_{16}-SAP	Saponite	50–60	86.6	Hexadecyltributylphosphonium cation	CO-OP Chemicals

Table 2. Composition and Characteristic Parameters of Various Nanocomposites

Samples	Type of OMLS	Clay (Inorganic Part) (wt %)	$M_w \times 10^{-3}$ (g/mol)	M_w/M_n
PBS	—	—	101	2.4
PBS/C_{18}-MMT	C_{18}-MMT	3.6	104	2.4
PBS/qC_{18}-MMT	qC_{18}-MMT	3.6	112	2.4
PBS/qC_{16}-SAP	qC_{16}-SAP	3.8	91	2.4

in the text) of the three different types of OMLS used in this research.

Nanocomposites Preparation

Nanocomposites were prepared with a twin-screw extruder (KZW15-30TGN, Technovel Corp.), operated at 150 °C. The first PBS/OMLS master batch was prepared throwing the OMLS powder from the window of the extruder barrel into the PBS melts. The prepared master batch and PBS pellets were dry-mixed by shaking them in a bag. The mixture was then melt-extruded with the same twin-screw extruder, operated at 150 °C, to yield nanocomposite strands. The color of the strands depends on the color of OMLS used. The composition and designation (as written in the text) of the prepared nanocomposites are presented in Table 2. The strands were pelletized and dried *in vacuo* at 75 °C for 7 h to remove water. Dried nanocomposites pellets were then converted into sheets with a thickness of 0.7–1.5 mm with a minimal compressive pressure (for the preparation of bubble-free nanocomposite sheets) at 135 °C for 3 min with a hot press. The molded sheets were then quickly quenched between glass plates and then annealed at 60 °C for 1.5 h to crystallize isothermally before being subjected to various characterizations (except for melt-rheological measurements). The content of inorganic parts in each nanocomposite was determined by burning sample pellets at 950 °C in a furnace.

Characterization Methods

Wide-Angle X-ray Diffraction (WAXD)

WAXD experiments were performed for three different types of OMLS powders and various nanocomposite sheets, respectively, with a Maxlabo X-ray diffractometer [MAC Science Co., 3 kW, graphite monochromator, Cu Kα radiation (wavelength: $\lambda = 0.154$ nm) operated at 40 kV/20 mA]. The samples were scanned in fixed time mode with a counting time of 2 s under the diffraction angle 2Θ in the range of 1–70°.

Transmission Electron Microscopy (TEM)

The morphology of various nanocomposites was investigated with a high-resolution TEM (H-7100, Hitachi Co.), operated at an accelerating voltage of 100 kV. The ultrathin sections (the edge of the sample sheets) with a thickness of 100 nm were microtomed at −80 °C with a Reichert Ultracut cryo-ultramicrotome without staining. The direction of compression mold relative to the TEM samples surface was perpendicular.

Gel Permeation Chromatography (GPC)

The number-average molecular weight (M_n) and weight-average molecular weight (M_w) of PBS matrix (before and after nanocomposites preparation) were determined with GPC (Jasco LC-2000plus system with Shodex K-804L column), with polystyrene standards for calibration and chloroform as a carrier solvent at 40 °C with a flow rate of 1 mL/min. The results of GPC measurements are summarized in Table 2. GPC data clearly indicated that there is almost no degradation of PBS matrix after nanocomposites preparation with various types of OMLS.

Dynamic Mechanical Analysis (DMA)

DMA of neat PBS and various nanocomposites were measured with a Rheometrics dynamic analyzer (RDAII) in the tension–torsion mode. The temperature dependence of the dynamic storage modulus (G'), loss modulus (G''), and their ratio ($\tan\delta$) were measured at a constant frequency (ω) of 6.28 rad $\cdot$ s^{-1}, a strain amplitude of 0.05%, and in the temperature range from −50 to 110 °C with a heating rate of 2 °C/min. The size of the test samples was 12 × 29 × 0.7 mm.

Tensile Properties

Dried PBS and various nanocomposites pellets were injection-molded with a minimixer as an injector (CSI, CS-183MMX) operated at 150 °C with out-of-control mold temperature. The tensile properties of injection-molded samples (crystallized at 60 °C for 1.5 h) were measured with an Instron 4505 (Instron Corp.) at 25 °C. The distance of chuck was 20 mm and the crosshead speed was 5 mm/min.

Measurement of O_2 Gas Permeability

The O_2 gas transmission rate of neat PBS and various nanocomposites was measured at 20 °C and 90% relative humidity by the ASTM D-1434 differential pressure method (GTR-30XAU, Yanaco Co.). Test samples were prepared by compression molding (thickness: ~300 μm), and melt-quenched samples were used for this measurement.

Melt Rheology

Melt rheological measurements were also conducted on an RDAII instrument with a torque transducer capable of measurements over the range of 0.2–200 g · cm. Dynamic oscillatory shear measurements were performed by applying a time-dependent strain of $\gamma(t) = \gamma_o \sin(\omega t)$, and the resultant shear stress was $\sigma(t) = \gamma_o[G' \sin(\omega t) + G'' \cos(\omega t)]$, with G' and G'' being the storage and loss moduli, respectively. Measurements were conducted with a set of 25-mm-diameter parallel plates with a sample thickness of ~1.5 mm and in the temperature range of 120–150 °C. The strain amplitude was fixed to 5% to obtain reasonable signal intensities even at elevated temperature or low ω to avoid the nonlinear response. For each nanocomposite investigated, the limits of linear viscoelasticity were determined by performing strain sweeps at a series of fixed ω's. The master curves were generated with the principle of time-temperature superposition and shifted to a common reference temperature (T_{ref}) of 120 °C, which was chosen as the most representative of a typical processing temperature of PBS.

Steady-shear viscosity measurements were conducted at 120 °C with a 25-mm-diameter cone and plate geometry with a cone angle of 0.1 rad. The steady-shear viscosity data reported in this article were obtained both as a function of shear rate and time. Before starting each experimental set, the sample was annealed at 120 °C for 5 min.

Biodegradability

The biodegradability of neat PBS and various nanocomposites was conducted in two different modes: under compost and under soil field.

Under Compost

In this mode biodegradability was examined on a homemade compost instrument at (58 ± 2) °C. The compost used was prepared from a mixture of soybean dust (byproduct of tofu) and effective microorganisms (EM-germ; purchased from Meikin CO-OP, Japan). Before use, this mixture was sealed and fermented for 20 days at open-air temperature. For this test the sample sheets (prepared with compression molding with a thickness of 0.3 ± 0.02 mm) were first clipped with a 35-mm slide holder and then put into the compost. After 35 days, samples were recovered from the compost, rinsed with distilled water, and finally washed with methanol with an ultrasonic bath for 5 min.

Under Soil Field

This test was carried out at Nagoya Municipal Research Institute (Nagoya, Japan) from March 15 to September 15, 2002. For this test we also used compression-molded sample sheets with an average thickness of 1 mm and each sheet weight of 3 ± 0.03 g. The sample sheets were first put into meshes net and then buried in the ground with leaf soil (the depth was ca. 15 cm).

RESULTS AND DISCUSSION

Nanocomposites Structure

The internal structure of the nanocomposite in the nanometer scale has typically been established with WAXD patterns and TEM observation. WAXD offers a convenient method to determine the interlayer spacing of the silicate layers in the original clay and in the intercalated polymer–clay nanocomposite. However, TEM allows a qualitative understanding of the dispersed clay structure through direct visualization.

Here, we combine both WAXD and TEM to understand the structure of PBS/OMLS nanocomposites in detail. The intercalation of polymer

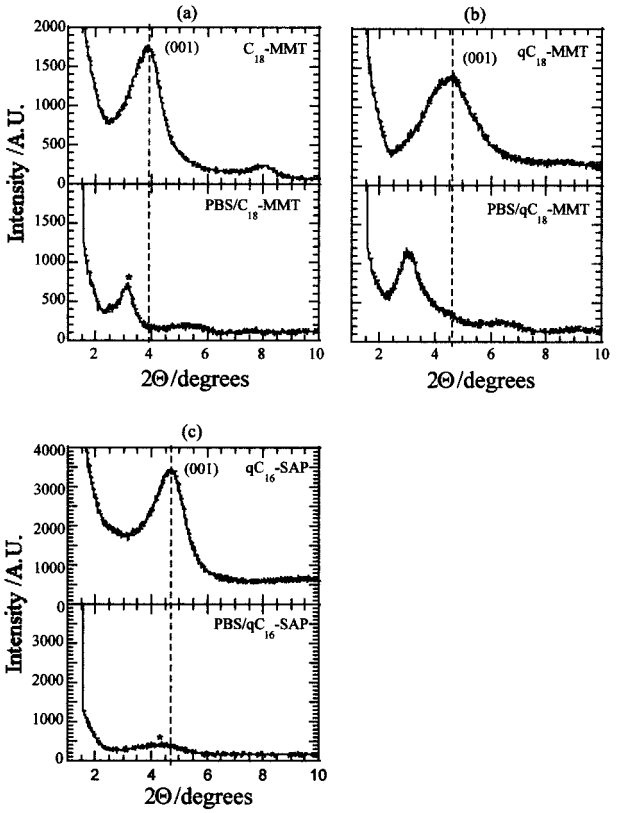

Figure 1. WAXD patterns for (a) pure C_{18}-MMT powder and corresponding nanocomposite with PBS, (b) pure qC_{18}-MMT powder and corresponding nanocomposite with PBS, and (c) pure qC_{16}-SAP powder and corresponding nanocomposite with PBS. The dashed line in each figure indicates the location of the silicate (001) reflection of OMLS, and asterisks indicate (001) peak of various OMLS dispersed in PBS matrix.

chains into the silicate galleries usually increases the interlayer spacing of OMLS as compared with the interlayer spacing of the pure OMLS, leading to a shift of the WAXD peak toward a lower value of 2Θ.

Figure 1(a) shows the results of WAXD analysis of pure C_{18}-MMT and the corresponding nanocomposite PBS/C_{18}-MMT in the range of 2Θ = 1–10°. The mean interlayer spacing of the C_{18}-MMT obtained by WAXD measurement was 2.31 nm (2Θ = 3.82°). In the case of nanocomposite, a sharp peak obtained at 2Θ = 3.15° (= 2.82 nm) indicates the formation of an intercalated structure but not well ordered because the width of the basal reflection of C_{18}-MMT decreases sharply after nanocomposite preparation. The width of the WAXD peak, β (measured by the full width at half-maximum), is inversely proportional to the coherence length of the scattering entities (D) and therefore reflects the coherent order of the silicate layers.[16,17] Because the width of the basal spacing of C_{18}-MMT decreased sharply after nanocomposite preparation with PBS, the coherency of the intercalated silicate layers was much higher than that of non-intercalated silicate layers. Thus, on the basis of WAXD analysis PBS melt intercalation had a strong effect on the layer structure of C_{18}-MMT, and significantly changed the coherence length of the silicate crystallites.

Figure 2(a) represents bright field TEM images of PBS/C_{18}-MMT nanocomposite of two different magnifications in which dark entities are the cross section of stacked intercalated C_{18}-MMT layers and bright areas are the matrix.[18] From the TEM images, we observed stacked and flocculated silicate layers, which were nicely distributed in the PBS matrix. The WAXD patterns of qC_{18}-MMT and corresponding nanocomposite are presented in Figure 1(b). Figure 2(b) is a bright field TEM image of fully intercalated PBS/qC_{18}-MMT nanocomposite with comparable magnification to the image of PBS/C_{18}-MMT nanocomposite as presented in Figure 2(a).

Therefore, from the WAXD analyses and TEM observations, it was confirmed that the extent of intercalation and the disruption of the original silicate structure occurred to a greater extent in the case of PBS/qC_{18}-MMT nanocomposite than that of PBS/C_{18}-MMT nanocomposite. Table 3 summarizes the form factors of various nanocomposites, that is, the average length (L_{clay}), thickness (d_{clay}) of the dispersed stacked intercalated silicate layers, and correlation length (ξ_{clay}) between them.

In contrast to PBS/C_{18}-MMT or PBS/qC_{18}-MMT nanocomposites, the WAXD pattern of PBS/qC_{16}-SAP nanocomposite [Fig. 1(c)] was almost featureless, only exhibiting a broad and extremely weak reflection at approximately 2Θ = 4.3°. The bright field TEM image of PBS/qC_{16}-SAP nanocomposite in two different magnifications is presented in Figure 2(c). Although the WAXD pattern is featureless, however, the delaminated and stacking structure of the silicate layers is readily observable, and this is more discernible with a high-magnification TEM image. Thus, the structure of PBS/qC_{16}-SAP nanocomposite represents stacked intercalated and delaminated silicate layers. The structure of the stacked silicate is nearly exfoliated, but the layered structure of silicate still remains.

On the basis of the WAXD patterns and TEM observations, three different types of nanocom-

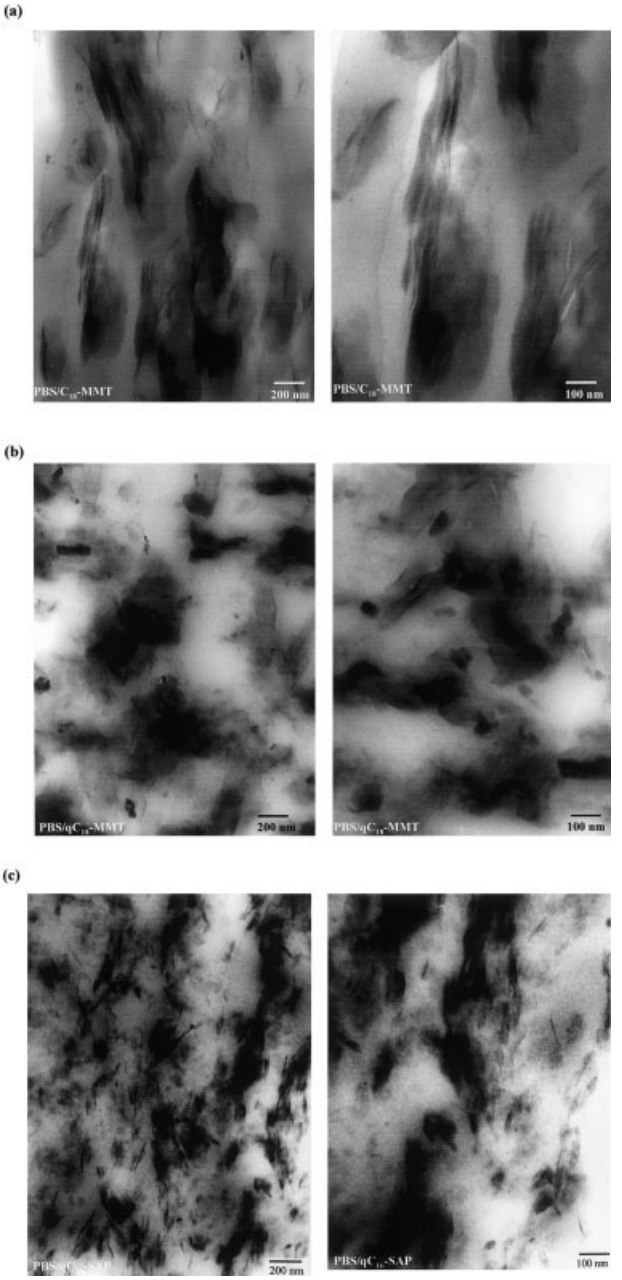

Figure 2. Bright field TEM images of (a) PBS/C_{18}-MMT nanocomposite, (b) PBS/qC_{18}-MMT nanocomposite, and (c) PBS/qC_{16}-SAP nanocomposite in which dark entities are the cross section of the intercalated or exfoliated silicate layers, and bright fields are the matrix.

posites were formed with three different types of OMLS. Intercalated and extended flocculated nanocomposite was observed in the case of the PBS/C_{18}-MMT system, intercalated and flocculated nanocomposite when qC_{18}-MMT was used as OMLS for nanocomposite preparation, whereas the coexistence of the stacked intercalated and delaminated structure was observed in PBS/qC_{16}-SAP nanocomposite.

Nanocomposite Properties

Dynamic Mechanical Analysis (DMA)

DMA measures the response of a given material to an oscillatory deformation (here, in the tension–torsion mode) as a function of temperature. The DMA results were expressed by three main parameters: (1) G' corresponding to the elastic response to the deformation, (2) G'' corresponding to the plastic response to the deformation, and (3) tan δ ($= G''/G'$), useful for determining the occurrence of molecular mobility transitions such as the glass-transition temperature (T_g).

DMA analysis has been used to track the temperature dependence of G', G'', and tan δ of neat PBS upon nanocomposites formation with three different types of OMLS. Figure 3 displays the temperature dependence of G', G'', and tan δ for neat PBS and the corresponding nanocomposites. For all nanocomposites, significant enhancement of G' was observed in the investigated temperature range, indicating intercalated PBS/OMLS nanocomposites have a strong effect on the elastic properties of the PBS matrix.

At the temperature range between -50 and 0 °C, the increments in G' were 197% for PBS/C_{18}-MMT, 178% for PBS/qC_{18}-MMT, and 116% for PBS/qC_{16}-SAP nanocomposite as compared to that of neat PBS. Furthermore, at the temperature range of 50–80 °C, all nanocomposites exhib-

Table 3. Form Factors of Nanocomposites Obtained from WAXD Analyses and TEM Observations

	PBS/C_{18}-MMT	PBS/qC_{18}-MMT	PBS/qC_{16}-SAP
WAXD			
d_{001}/nm	2.82	2.88	2.14
Δd_{001}^{a}	0.51	0.95	0.27
D/nm[b]	15.3	13.3	7.20
D/d_{001}	5.56	4.61	3.36
TEM			
L_{clay}	1721 ± 15	738 ± 60	367 ± 13
ξ_{clay}	69 ± 29	72 ± 27	54 ± 43
L_{clay}/D	≈112	≈56	≈50

[a] Extent of intercalation, and can be defined as Δd_{001} ($d_{nanocomposite}$-d_{OMLS}).
[b] Calculated on the basis of the Scherrer equation.[12]

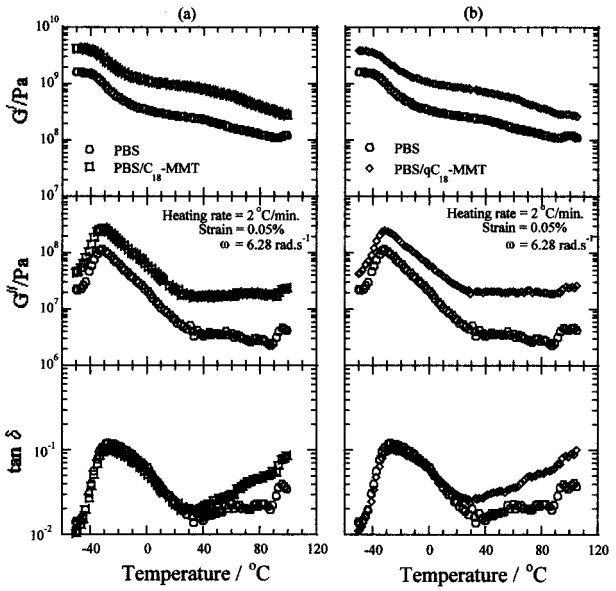

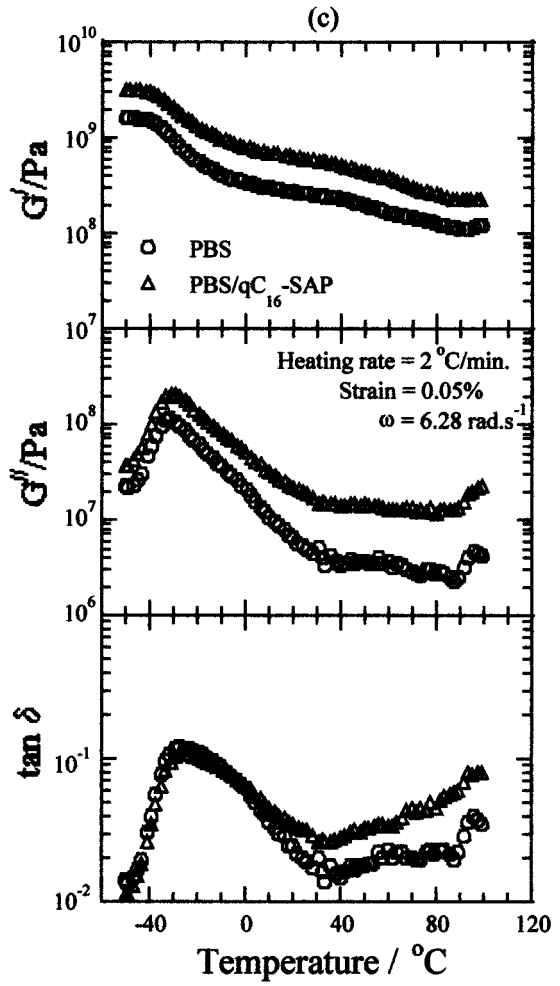

Figure 3. Temperature dependence of G', G'', and their ratio tan δ for neat PBS and various nanocomposites. (a) PBS/C_{18}-MMT nanocomposite, (b) PBS/qC_{18}-MMT nanocomposite, and (c) PBS/qC_{16}-SAP nanocomposite.

ited much higher enhancement in G' (249% for PBS/C_{18}-MMT, 214% for PBS/qC_{18}-MMT, and 120% for PBS/qC_{16}-SAP nanocomposites) than that of neat PBS. This was due to both mechanical reinforcement by clay particles[19] and extended intercalation[20] at high temperature. Above the T_g, when materials become soft, the reinforcement effect of the clay particles becomes prominent because of restrict movement of the polymer chains; hence, strong enhancement appears.

Among the three nanocomposites, PBS/C_{18}-MMT nanocomposite exhibits very high enhancement of modulus for all temperature ranges. Table 4 summarizes the G' values of three different nanocomposites and neat PBS at various temperature ranges. The essential factor governing the enhancement of mechanical properties is the aspect ratio of the dispersed intercalated clay particles.[21] From the TEM images (see Fig. 2) and Table 3, there is a strong flocculation of the dispersed intercalated silicate layers because of the edge–edge interaction of the clay particles for PBS/C_{18}-MMT nanocomposite.[4–6] For this reason, the length of the dispersed clay particles increase significantly and ultimately increase in a two-dimensional aspect ratio.[14]

However, above T_g the enhancement of G'' is much higher in the intercalated nanocomposites as compared with that of below T_g, indicating the plastic response to the deformation is prominent in the presence of OMLS when materials become soft. However, the presence of OMLS does not lead to a significant shift and broadening of the tan δ curves for all nanocomposites as compared with that of neat PBS. This behavior has been ascribed to the restricted segmental movements at the organic–inorganic interface neighborhood of intercalated PBS-nanocomposites.

Table 4. G' of Neat PBS and Various Nanocomposites in Different Temperature Ranges

	G'/GPa			
Samples	−50 °C	0 °C	50 °C	100 °C
PBS	1.6	0.34	0.20	0.19
PBS/C_{18}-MMT	4.3	1.10	0.69	0.27
PBS/qC_{18}-MMT	3.9	1.05	0.63	0.28
PBS/qC_{16}-SAP	3.2	0.79	0.43	0.22

Table 5. Tensile Properties and O_2 Gas Permeability of Neat PBS and Nanocomposites

Properties	PBS	PBS/C_{18}-MMT	PBS/qC_{18}-MMT	PBS/qC_{16}-SAP
Tensile yield strength/MPa	35	34.2	32.5	31.6
Tensile modulus/GPa	0.53	0.88	0.82	0.71
O_2 gas permeability coefficient/ (mL · mm/m^2 · day · MPa)	87.3	42.2	69.0	71.2

Tensile Properties

Table 5 reports the tensile strength and modulus of neat PBS and various nanocomposites. There was a significant increase for PBS/C_{18}-MMT nanocomposite as compared with that of neat PBS and various other nanocomposites. This behavior again was due to the higher aspect ratio of dispersed clay particles in the case of PBS/C_{18}-MMT nanocomposite. The aspect ratio of dispersed clay particles in various nanocomposites follows PBS/C_{18}-MMT > PBS/qC_{18}-MMT > PBS/qC_{16}-SAP, and the final modulus follows the same order. However, the tensile strengths of various nanocomposites are almost the same or somewhat low as compared with that of neat PBS. This behavior may be due to a weak interaction between polymer matrix and OMLS.[12]

O_2 Gas Permeability

The layered silicates are believed to increase the gas-barrier properties by creating a maze or tortuous path that retards the progress of gas molecules through the matrix resin.[9,10,12,22–24] The O_2 gas permeability for the neat PBS and various nanocomposites is presented in Table 5. According to the Nielsen model,[25] platelets of length ($\cong L_{clay}$) and width ($\cong D_{clay}$) of the clay, which are dispersed parallel in a polymer matrix, and the tortuosity factor (τ) can be expressed as

$$\tau = 1 + (L_{clay}/2D_{clay})\phi_{clay} \quad (1)$$

where ϕ_{clay} is the volume fraction of dispersed clay particles. Therefore, the relative permeability coefficient (P_{PBSCN}/P_{PBS}) is given by

$$\frac{P_{PBSCN}}{P_{PBS}} = \tau^{-1} = \frac{1}{1 + (L_{clay}/2D_{clay})\phi_{clay}} \quad (2)$$

where P_{PBSCN} and P_{PBS} are the permeability coefficients of PBS/OMLS nanocomposites and neat PBS, respectively. We considered PBS/C_{18}-MMT nanocomposite to confirm the validity of the aforementioned model in the case of these nanocomposite systems, with the value of L_{clay} = 1721 nm (from TEM images) and the value of D_{clay} = 15.3 nm as calculated with Scherrer's equation.[16,17] Therefore, the calculated value of P_{PBSCN}/P_{PBS} for PBS/C_{18}-MMT nanocomposite was equal to 0.55. The experimental value of 0.48 was almost well matched with the preceding model but slightly lower than the calculated one. This behavior may be due to the high degree of crystallinity in the case of nanocomposites in the presence of clay as compared to that of neat PBS, as in nanocomposite clay particles acting as a nucleator for crystallization.[20]

Melt Rheology

The measurement of rheological properties of polymeric materials under a molten state is crucial to gain a fundamental understanding of the nature of the processability and the structure–property relationship for these materials.

Dynamic Oscillatory Shear

The linear viscoelastic master curves for the neat PBS and three different nanocomposites are displayed in Figure 4. The master curves were generated by applying the time-temperature superposition principle and shifted to a T_{ref} of 120 °C with both a_T and the vertical shift factor (b_T).

Figure 4 demonstrates that both moduli of nanocomposites increase monotonically at all frequencies as compared to that of neat PBS. At high frequencies (>10 rad · s^{-1}), the viscoelastic behaviors of all nanocomposites are the same, with the exception of only a systematic increase in the modulus value. However, at low frequencies (<10

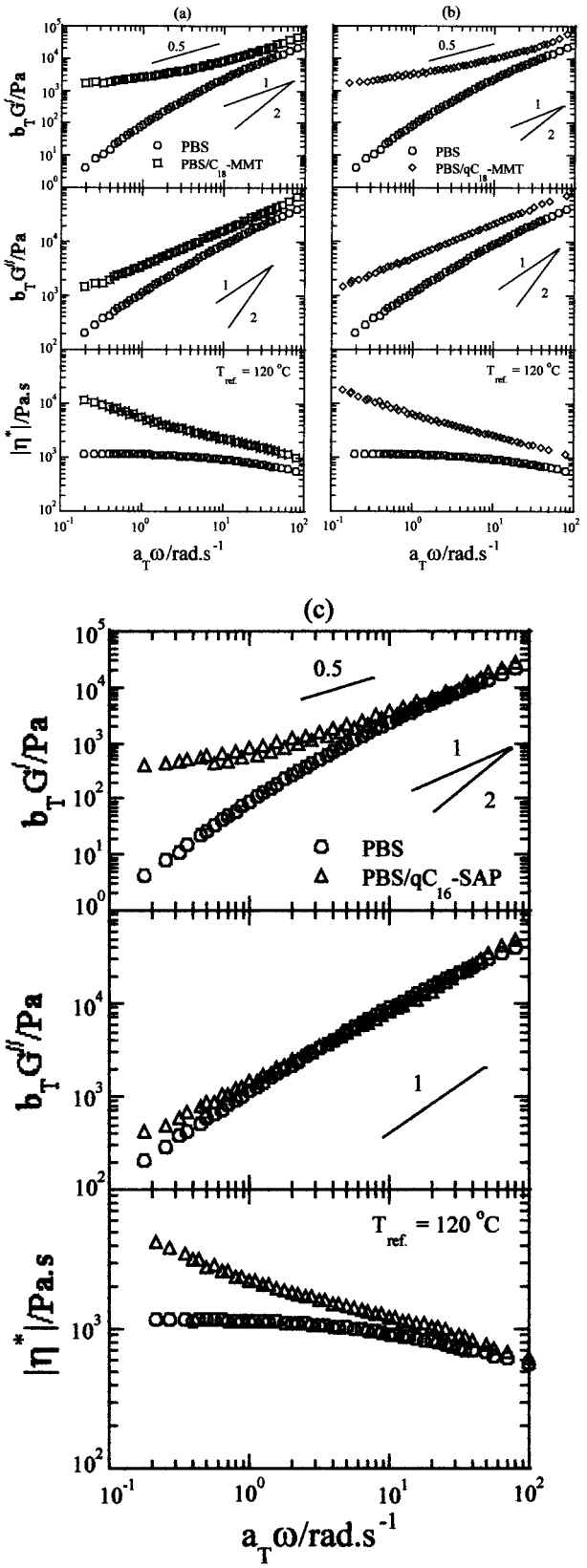

Table 6. Terminal Region Slopes (<10 rad $\cdot$ s^{-1}) of G' and G'' of PBS and Nanocomposites

Samples	G'	G''
PBS	1.7	1.0
PBS/C_{18}-MMT	0.2	0.4
PBS/qC_{18}-MMT	0.25	0.6
PBS/qC_{16}-SAP	0.3	0.7

rad $\cdot$ s^{-1}), both moduli of nanocomposites exhibit weak frequency dependence, meaning there is a gradual change of behavior from liquidlike ([$G' \propto \omega^2$ and $G'' \propto \omega$]) to solidlike with the incorporation of clay in the PBS matrix.

The terminal region slopes of both moduli of neat PBS and three different nanocomposites were estimated at low frequencies (<10 rad $\cdot$ s^{-1}) and are presented in Table 6. The lower slope values and the higher absolute values of the dynamic moduli indicated the formation of a spatially linked structure (also observed from TEM photographs) in the nanocomposites under the molten state.[4–6,26,27] Because of this structure or highly geometric constraints, the individual stacked silicate layers were incapable of freely rotating; hence, by imposing small $a_T\omega$ the relaxations of the structure were prevented almost completely. This type of prevented relaxation due to the highly geometric constraints of the stacked and intercalated silicate layers led to the presence of the solidlike behavior as observed in nanocomposites.[28] The degree of this prevented relaxation was greater for the PBS/C_{18}-MMT nanocomposite because of the presence of the strongly flocculated structure. For this reason, the $G'(\omega)$ curve showed some frequency independence in the low-frequency region.

The dynamic complex viscosity [$|\eta^*|(\omega)$] master curves for the neat PBS and nanocomposites, based on linear dynamic oscillatory shear measurements, are also shown in Figure 4. In the low-frequency region the neat PBS exhibited almost Newtonian behavior, whereas all nanocomposites exhibited a very strong shear-thinning tendency. We believe this behavior comes from

Figure 4. Reduced-frequency dependence of $G'(\omega)$, $G''(\omega)$, and $|\eta^*|(\omega)$ of neat PBS and various nanocomposites: (a) PBS/C_{18}-MMT nanocomposite, (b) PBS/qC_{18}-MMT nanocomposite, and (c) PBS/qC_{16}-SAP nanocomposite.

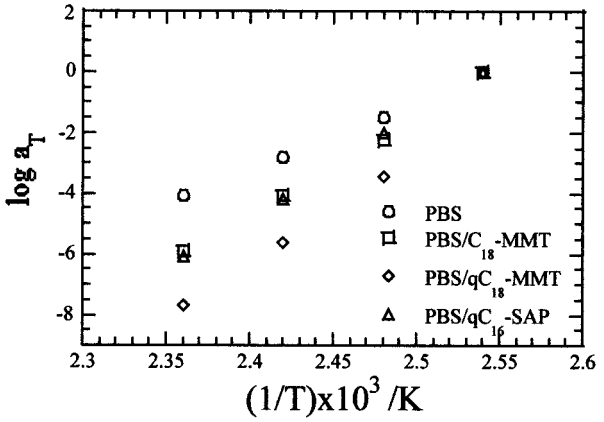

Figure 5. Frequency shift factors (a_T) as a function of temperature of neat PBS and various nanocomposites.

the nature of the clay particles, which were dispersed in the PBS matrix.

In our previous study on lyophilized smectic clay-toluene suspensions,[29] we observed this type of shear-thinning feature of the clay particles in the rapid shear flow. Such a feature was strongly dependent on the shear rate in the dynamic measurements because of the formation of the shear-induced alignment of the dispersed clay particles.

The temperature-dependence frequency shift factors (a_T, Arrhenius type) used to generate master curves shown in Figure 4 are portrayed in Figure 5. The dependence of the frequency shift factors on the silicate loading suggested that the temperature-dependent relaxations process observed in the viscoelastic measurements are somehow affected in the presence of silicate layers.[14,30]

Steady Shear

The steady-shear rheological behavior of neat PBS and a series of nanocomposites is displayed in Figure 6. The shear viscosity of nanocomposites was enhanced considerably at all shear rates with time and increased monotonically with a decreasing shear rate. However, all nanocomposites exhibited strong rheopexy behavior, and this behavior became prominent at low shear rates (0.001 s^{-1}), whereas neat PBS exhibited a time-independent viscosity at all shear rates. With increasing shear rates, the shear viscosity was attained plateau after a certain time, and the time require to attain this plateau decreased with increasing shear rates. The reason for this type of behavior may be due to the planer alignment of the clay particles toward the flow direction under shear. When the shear rate is very slow (0.001 s^{-1}), clay particles take longer to attain complete planer alignment along the flow direction, and this measurement time (1000 s) is too short to

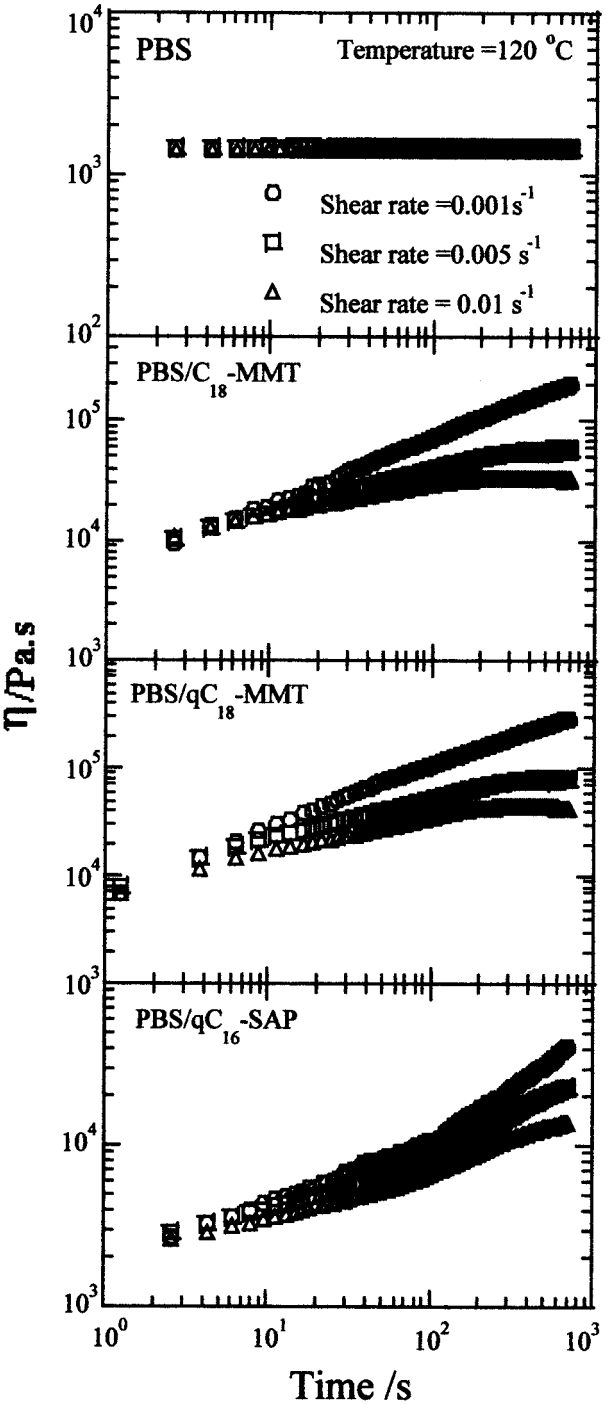

Figure 6. Steady-shear viscosity (η) of neat PBS and various nanocomposites as a function of time.

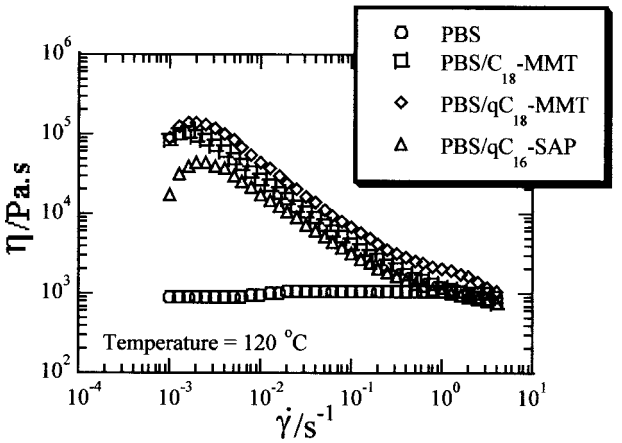

Figure 7. η of neat PBS and various nanocomposites as a function of shear rates.

attain such an alignment and shows strong rheopexy behavior. However, under small higher shear rates of 0.005 or 0.01 s^{-1}, this measurement time was sufficient to attain such alignment, and nanocomposites showed time-independent shear viscosity after a certain time.

Figure 7 displays the shear-rate dependence on the viscosity for neat PBS and various nanocomposites measured at 120 °C. The neat PBS exhibited Newtonian behavior at all shear rates, whereas nanocomposites exhibited non-Newtonian behavior. At very low shear rates, the shear viscosity of nanocomposites initially exhibited some shear-thickening behavior, and this corresponded to the rheopexy as observed at very low shear rates (see Fig. 6). After that, all PBSCNs showed very strong shear-thinning behavior at all measured shear rates, and this behavior was analogous to the results obtained in the case of oscillatory shear measurements (see Fig. 4). Additionally, at very high shear rates, the steady-shear viscosities of nanocomposites were comparable to that of neat PBS. These observations suggested that the silicate layers are strongly oriented toward the flow direction at high shear rates, and shear-thinning behavior at high shear rates is dominated by that of neat PBS.[14,31]

Biodegradability

We also investigated the biodegradability of neat PBS before and after nanocomposites preparation with three different types of OMLS. We used alkylammonium or alkylphosphonium salts for the modification of pristine layered silicates, and these surfactants are toxic for microorganisms. Lee et al.[32] first reported on the biodegradability of aliphatic polyester (BAP) on the basis of nanocomposites under compost. Very recently, Maiti et al.[33] reported the biodegradability of the poly(hydroxybutyrate) (PHB)/OMLS nanocomposite system. Both groups of researchers assumed the retardation of biodegradation of BAP or PHB because of the improvement of the barrier properties of the matrices after nanocomposites preparation with OMLS. However, they did not report anything about the permeability. However, in the case of PLACNs we did not find any relation be-

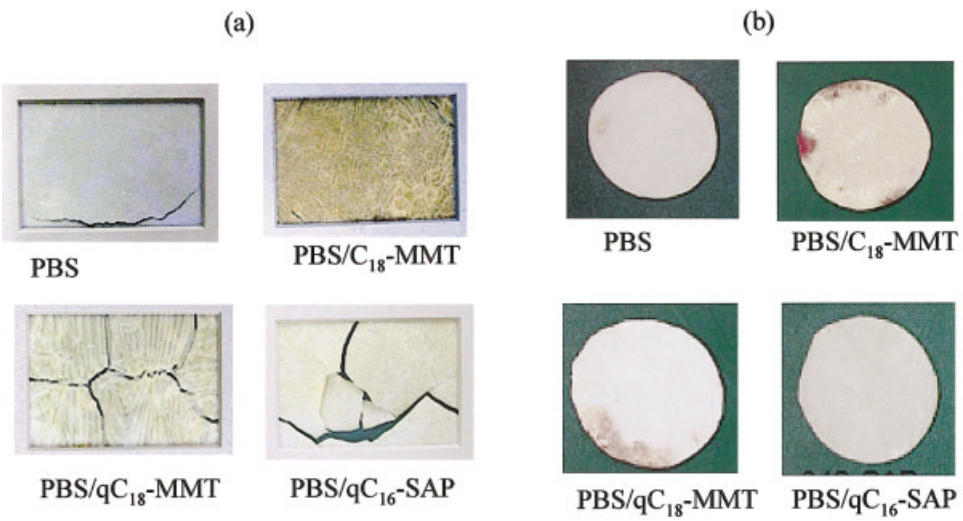

Figure 8. Biodegradability of neat PBS and various nanocomposites sheets (a) under compost and (b) under soil field.

Table 7. GPC Results of Various Samples Recovered from Compost after 35 Days

Samples	$M_w \times 10^{-3}$ (g/mol)	$M_n \times 10^{-3}$ (g/mol)	$M_w^o \times 10^{-3}$ (g/mol)	M_w/M_w^o
PBS	16	3.8	101	0.16
PBS/C_{18}-MMT	17	6.6	104	0.16
PBS/qC_{18}-MMT	17	4.4	112	0.15
PBS/qC_{16}-SAP	8.7	1.2	91	0.096

M_w^o is the molecular weight before composting.

tween the biodegradability and the gas-barrier properties. Some PLACNs degraded very fast having significantly improved barrier properties as compared with that of neat PLA.[9,10]

Figure 8(a) shows the real pictures of recovered samples of neat PBS and various nanocomposites from the compost after 35 days. Many cracks appeared in nanocomposite samples as compared to that of neat PBS. This observation indicated the improved degradability of nanocomposites in compost. This kind of fracture has an advantage for biodegradation because it is easy to mix with compost and create much more surface area for further attack by microorganisms, and the extent of fragmentation is directly related to the nature of OMLS used for nanocomposites preparation. We also conducted the GPC measurement of recovered samples from compost, and we discovered that the extent of molecular weight loss was almost the same for all samples (see Table 7). This result indicated that the extent of hydrolysis of PBS in the pure state or OMLS-filled systems is the same in compost.

Except for the PBS/qC_{16}-SAP system, the degree of degradation was not different for other samples. This observation indicated that montmorillonite or alkylammonium cations, as well as other properties, has no effect on the biodegradability of PBS. The accelerated degradation of PBS matrix in the presence of qC_{16}-SAP may be due to the presence of alkylphosphonium surfactant. This kind of behavior was also observed in the case of PLA/OMLS nanocomposite systems.[11,34]

It is very difficult for us to propose the exact mechanism of the compost degradability of PBS because these are our preliminary results, and in our forthcoming research,[35] we will try to describe the compost degradability of PBS and corresponding nanocomposites.

We also observed the nature of degradation of PBS and various nanocomposites under soil field. This experiment was conducted for 1, 2, and 6 months. After 1 and 2 months, there was no change in the nature of the sample surfaces, but after 6 months black or red spots appeared on the surface of the nanocomposites samples. Figure 8(b) represents the results of degradation of neat PBS and various nanocomposites sheets recovered from a soil field after 6 months. We believe these spots on the sample surface were due to the fungus attacked because when we put these parts into the slurry, we observed clear growth of fungus. These results also indicated that nanocomposites exhibit the same or a higher level of biodegradability as compared with the PBS matrix.

CONCLUSIONS

We prepared a series of novel biodegradable PBS/layered silicate nanocomposites by simple melt extrusion of PBS pellets and three different types of OMLS powders. The silicate layers were either intercalated and flocculated or the coexistence of intercalated and exfoliated, and were nicely distributed in the PBS matrix. The materials properties of PBS were significantly improved after nanocomposites preparation with various kinds of OMLS and completely depended on the nature of OMLS. These concurrent properties of improvement were well beyond what can be generally achieved through the micro/macrocomposites preparation[2,36] or chemical modification of neat PBS.[37]

Thanks are due to the Japan Society for the Promotion of Science (JSPS) for awarding a Postdoctoral Fellowship and a research grant to S. Sinha Ray (P02152).

REFERENCES AND NOTES

1. Narayan, R. Degradation of Polymeric Materials. In Science and Engineering of Composting: Envi-

ronmental, Microbiology and Utilization Aspects; Hoitink, H. A.; Keener, H. N., Eds.; OARDC: Wooster, Ohio, 1993.
2. Ratto, J. A.; Stenhouse, P. J.; Auerbach, M.; Mitchel, J.; Farell, R. Polymer 1999, 40, 6777–6788, and the references cited therein.
3. Fujimaki, T. Polym Degrad Stab 1998, 59, 209–214.
4. Sinha Ray, S.; Maiti, P.; Okamoto, M.; Yamada, K.; Ueda, K. Macromolecules 2002, 35, 3104–3110.
5. Sinha Ray, S.; Okamoto, K.; Yamada, K.; Okamoto, M. Nano Lett 2002, 2, 423–426.
6. Sinha Ray, S.; Yamada, K.; Okamoto, M.; Ogami, A.; Ueda, K. Compos Interfaces, 2003, 10, 435–450.
7. Sinha Ray, S.; Yamada, K.; Okamoto, M.; Ueda, K. Nano Lett 2002, 2, 1093–1096.
8. Sinha Ray, S.; Yamada, K.; Okamoto, M.; Ueda, K. Polymer 2003, 44, 857–866.
9. Sinha Ray, S.; Yamada, K.; Ogami, A.; Okamoto, M.; Ueda, K. Macromol Rapid Commun 2002, 23, 943–947.
10. Sinha Ray, S.; Yamada, K.; Okamoto, M.; Ogami, A.; Ueda, K. Chem Mater 2003, 15, 1456–1465.
11. Sinha Ray, S.; Yamada, K.; Okamoto, M.; Ueda, K. Macromol Mater Eng 2003, 288, 203–208.
12. Sinha Ray, S.; Okamoto, M. Prog Polym Sci, in press.
13. Sinha Ray, S.; Okamoto, K.; Maiti, P.; Okamoto, M. J Nanosci Nanotech 2002, 2, 171–176.
14. Sinha Ray, S.; Okamoto, K.; Okamoto, M. Macromolecules 2003, 36, 2355–2376.
15. Yasuda, T.; Takiyama, E. U.S. Patent 5 391 644, 1995.
16. $D = (\lambda k)/(\beta \cos\theta)$, where k is a constant and generally equal to 0.9, $\lambda = 0.154$ nm, and θ is the WAXD peak position.
17. Dritis, V. A.; Tchoubar, C. X-ray Diffraction by Disordered Lamellar Structures; Springer-Verlag: New York, 1990; Vol. 90, pp 21–22.
18. Because the silicate layers are comprised of heavier elements (Al, Si, and O) than the interlayer and surrounding matrix (C, H, N, etc.), they appear darker in bright field images.
19. Usuki, A.; Kawasumi, M.; Kojima, Y.; Okada, A.; Kurauchi, T.; Kamigaito, O. J Mater Res 1993, 8, 1185–1188.
20. Maiti, P.; Nam, P. H.; Okamoto, M.; Usuki, A.; Hasegawa, N. Macromolecules 2002, 35, 2042–2049.
21. Nam, P. H.; Maiti, P.; Okamoto, M.; Kotaka, T.; Hasegawa, N.; Usuki, A. Polymer 2001, 42, 9633–9640.
22. Yano, K.; Usuki, A.; Okada, A.; Kurachi, T.; Kamigaito, O. J Polym Sci Part A: Polym Chem 1993, 31, 2493–2498.
23. Xu, R.; Manias, E.; Snyder, A. J.; Runt, J. Macromolecules 2001, 34, 337–339.
24. Bharadwaj, R. K. Macromolecules 2001, 34, 9189–9191.
25. Nielsen, L. J Macromol Sci Chem 1967, 1, 929–935.
26. Ren, J.; Silva, A. S.; Krishnamoorti, R. Macromolecules 2000, 33, 3739–3746.
27. Galgali, G.; Ramesh, C.; Lele, A. Macromolecules 2001, 34, 852–856.
28. Hoffmann, B.; Kressler, J.; Stoppelmass, G.; Friedrich, Chr.; Kim, G. M. Colloid Polym Sci 2000, 278, 629–636.
29. Okamoto, M.; Taguchi, H.; Sato, H.; Kotaka, T.; Tatayama, H. Langmuir 2000, 16, 4055–4058.
30. Krisnhamoorti, R.; Giannelis, E. P. Macromolecules 1997, 30, 4097–4102.
31. Krishnamoorti, R.; Ren, J.; Silva, A. S. J Chem Phys 2001, 114, 4968–4973.
32. Lee, S. R.; Park, H. M.; Lim, H.; Kang, T.; Li, X.; Cho, W. J. Polymer 2002, 43, 2495–2500.
33. Maiti, P.; Batt, C. A.; Giannelis, E. P. Polym Mater Sci Eng 2003, 88, 58–59.
34. Sinha Ray, S.; Yamada, K.; Okamoto, M.; Ogami, A.; Ueda, K. Polymer, 2003, 44, 6633–6646.
35. Sinha Ray, S.; Okamoto, K.; Okamoto, M. J Mater Chem, manuscript submitted for publication, 2003.
36. Mani, R.; Bhattacharya, M. Eur Polym J 2001, 37, 515–526, and the references cited therein.
37. Mani, R.; Bhattacharya, M.; Tang, J. J Polym Sci Part A: Polym Chem 1999, 37, 1693–1702.